Journal of Mathematical Imaging and Vision, 13, 1–19 (2000)

On the Fourier Properties of Discontinuous Motion

STEVEN S. BEAUCHEMIN
GRASP Laboratory, University of Pennsylvania, Philadelphia PA 19104-6228, USA

JOHN L. BARRON
The University of Western Ontario, London, Canada N6A 5B7

;

Abstract. Retinal image motion and optical flow as its approximation are fundamental concepts in the field of vision, perceptual and computational. However, the computation of optical flow remains a challenging problem as image motion includes discontinuities and multiple values mostly due to scene geometry, surface translucency and various photometric effects such as reflectance. In this contribution, we analyze image motion in the frequency space with respect to motion discontinuities and translucence. We derive the frequency structure of motion discontinuities due to occlusion and we demonstrate its various geometrical properties. The aperture problem is investigated and we show that the information content of an occlusion almost always disambiguates the velocity of an occluding signal suffering from the aperture problem. In addition, the theoretical framework can describe the exact frequency structure of Non-Fourier motion and bridges the gap between Non-Fourier visual phenomena and their understanding in the frequency domain.

Keywords: Image motion, optical flow, occlusion, aperture problem, non-Fourier motion

1. Introduction

A fundamental problem in processing sequences of images is the computation of *optical flow*, an approximation to image motion defined as the projection of velocities of 3D surface points onto the imaging plane of a visual sensor. The importance of motion in visual processing cannot be understated: in particular, approximations to image motion may be used to estimate 3D scene properties and motion parameters from a moving visual sensor [21, 30, 31, 42, 51, 50, 1, 5, 38, 22, 54, 56, 34, 20, 16, 23], to perform motion segmentation [7, 40, 45, 36, 47, 14, 25, 8, 2, 46, 15], to compute the focus of expansion and time-to-collision [44, 41, 48, 24, 49, 9], to perform motion-compensated image encoding [10, 13, 35, 37, 39, 55], to compute stereo disparity [3, 12, 26, 28], to measure blood flow and heart-wall motion in medical imagery [43], and, recently, to measure minute amounts of growth in corn seedlings [6, 29].

1.1. Organization of Paper

This contribution addresses the problem of multiple image motions arising from occlusion and translucency phenomena. We present a theoretical framework for discontinuous optical flow in the Fourier domain. The concept of image velocity as a geometric function is described in Section 1.

Section 2 is an analysis of occlusion in Fourier space with a constant model of velocity. Our approach focuses on the frequency structure of occluding surfaces and the theoretical results are constructed incrementally. For instance, a simple model of velocity is used to develop the structure of occlusion with sinusoidal signals which are then generalized to arbitrary signals. These theoretical results demonstrate that occlusion may be differentiated from translucency and the motions associated with both the occluding and occluded surfaces can be discriminated.

Section 3 is an investigation of the aperture problem and degenerate[1] signals, as they appear in the theoretical framework. For example, it is shown that the full velocity of a degenerate signal is almost always computable at the occlusion.

Section 4 is a study of related issues such as translucency phenomena, Non-Fourier motion, generalized occlusion boundaries and phase shifts. Numerical experiments supporting the framework are presented. Results obtained with sets of sinusoidal signals created synthetically are compared with their corresponding theoretical predictions. Section 5 summarizes our results.

1.2. Contribution

The motivation for the theoretical framework emanates from the observation that occlusion and translucency in the context of computing optical flow constitute difficult challenges and threatens its precise computation. The theoretical results cast light on the exact structure of occlusion and translucency in the frequency domain.

The results are essentially theoretical and stated in the form of Theorems and Corollaries. Relevant numerical experiments which support the theoretical results are presented. In addition, this contribution bridges what is seen as an important gap between Non-Fourier models of visual stimuli and optical flow methods in Computer Vision. In fact, Non-Fourier visual stimuli, to which belong translucency and occlusion effects, have been studied mainly with respect to the motion percept these stimuli elicit among human subjects [11, 52, 53]. However, more recently, it has been conjectured that a viable computational analysis of Non-Fourier motion could be carried out with Fourier analysis, since many Non-Fourier stimuli turn out to have simple frequency characterizations [19]. The results presented herein extend the concept of Non-Fourier stimuli such as occlusion and translucency from being not at all explained by its Fourier characteristics to the establishment of exact frequency models of visual stimuli exhibiting occlusions and translucencies.

As a first attempt to understand occlusion, the simplest set of controllable parameters were used, such as the structure of occlusion boundaries and the number of distinct frequencies for representing the occluding and occluded surfaces. A constant model of velocity was also used and no signal deformations (such as those created by perspective projection) were permitted. These preliminary results are extended to image signals composed of an arbitrary number of discrete frequencies. Dirichlet conditions are hypothesized for each signal thus allowing to expand them as complex exponential series.

The potential use of the information-content of an occlusion boundary is outlined. Occluding boundaries contain a wealth of information that is not exploited by conventional optical flow frameworks, due to a theoretical void. It is shown that a degenerate occluding signal exhibiting a linear spectrum is supplemented by the linear orientation of its occluding boundary. These two spectra almost always yield the full velocity of an occluding signal suffering from the aperture problem. The structure of occlusion when both signals are degenerate is also shown. It is demonstrated that this particular case collapses to a one-dimensional structure.

The Corollaries show that additive translucency phenomena may be understood as a special case of the theoretical framework. In addition, the velocities associated with both the occluding and occluded signals may be identified as such, without the need of scenic information such as depth.

1.3. Image Motion

Image motion is expressed in terms of the 3D motion parameters of the visual sensor and the 3D environmental points of the scene: let $\mathbf{P}^T = (X, Y, Z)$ be an environmental point, $\mathbf{\Omega}^T = (\Omega_x, \Omega_y, \Omega_z)$ and $\mathbf{T}^T = (T_x, T_y, T_z)$ be the visu-

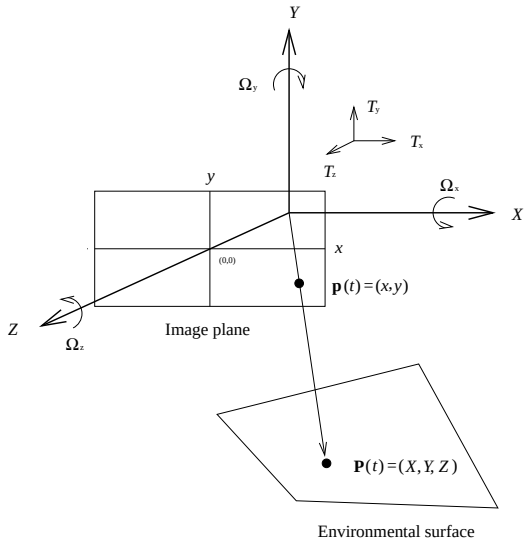

Fig. 1. The geometry of the visual sensor. $\mathbf{\Omega}^T = (\Omega_x, \Omega_y, \Omega_z)$ *and* $\mathbf{T}^T = (T_x, T_y, T_z)$ *are the instantaneous rotation and translation of the visual sensor.* $\mathbf{p}(t)$ *is the perspective projection of* $\mathbf{P}(t)$ *onto the imaging surface.*

al sensor's respective instantaneous rate of change in rotation and translation and $\mathbf{p} = \frac{\mathbf{P}}{\mathbf{P}\cdot\hat{\mathbf{z}}}$ the perspective projection of $\mathbf{P}$ onto the imaging surface (the focal length of the sensor is assumed to be 1), where $\hat{\mathbf{z}}$ is a normalized vector along the line-of-sight axis Z. The setup is shown in Figure 1. The instantaneous 3D velocity of $\mathbf{P}$ is given by

$$\mathbf{V} = -\mathbf{T} - \mathbf{\Omega} \times \mathbf{P}. \tag{1}$$

The relationship between the 3D motion parameters and 2D velocity that results from the projection of $\mathbf{V}$ onto the image plane can be obtained by temporally differentiating $\mathbf{p}$:

$$\mathbf{v}(\mathbf{x}) \stackrel{\text{def}}{=} \dot{\mathbf{p}} = \begin{pmatrix} \frac{\dot{X}}{Z} - \frac{X\dot{Z}}{Z^2} \\ \frac{\dot{Y}}{Z} - \frac{Y\dot{Z}}{Z^2} \end{pmatrix}. \tag{2}$$

Using $\mathbf{V}^T \stackrel{\text{def}}{=} (\dot{X}, \dot{Y}, \dot{Z}) = (-T_x - \Omega_y Z + \Omega_z Y, -T_y - \Omega_z X + \Omega_x Z, -T_z + \Omega_x Y - \Omega_y X)$ for substitution in (2), one obtains the image velocity equation [31]:

$$\begin{aligned} \mathbf{v}(\mathbf{x}) &= \begin{pmatrix} Z^{-1}(xT_z - T_x) \\ Z^{-1}(yT_z - T_y) \end{pmatrix} \\ &+ \begin{pmatrix} xy\Omega_x - (1+x^2)\Omega_y + y\Omega_z \\ (1+y^2)\Omega_x - xy\Omega_y - x\Omega_z \end{pmatrix}. \end{aligned} \tag{3}$$

Hence, image motion is a purely geometric quantity and, consequently, for optical flow to be exactly image motion, a number of conditions have to be satisfied. These are: *a) uniform illumination; b) Lambertian surface reflectance* and *c) pure translation parallel to the image plane.* Realistically, these conditions are never entirely satisfied in scenery. Instead, it is assumed that these conditions hold locally in the scene and therefore locally on the image plane. The degree to which these conditions are satisfied partly determines the accuracy with which optical flow approximates image motion.

1.4. Multiple Motions

Given an arbitrary environment and a moving visual sensor, the motion field generated onto the imaging plane by a 3D scene within the visual field is represented as function (3) of the motion parameters of the visual sensor. Discontinuities in image motion are then introduced in (3) whenever the depth Z is other than single-valued and differentiable[2]. The occurrence of occlusion causes the depth function to exhibit a discontinuity, whereas translucency leads to a multiple-valued depth function.

1.5. Models of Optical Flow

Generally, the optical flow function may be expressed as a polynomial in some local coordinate system of the image space of the visual sensor. It is assumed that the center of the neighborhood coincides with the origin of the local coordinate system. In this case, we may write the Taylor series expansion of a i^{th} velocity about the origin as:

$$\mathbf{v}_i(\mathbf{x},t) = \sum_{j=0}^{p}\sum_{k=0}^{q}\sum_{l=0}^{r}\frac{\partial^{j+k+l}\mathbf{v}_i}{j!k!l!\partial x^j\partial y^k\partial t^l}x^j y^k t^l \Bigg|_{\mathbf{x},t=\mathbf{0}} \quad (4)$$

where $p+q+r \leq n$. However, we simply adopt in what follows Fleet and Jepson's [18] constant model of optical flow denoted as:

$$\mathbf{v}_i(\mathbf{x},t) = \mathbf{x} - \mathbf{a}_i t, \quad (5)$$

where $\mathbf{a}_i$ is now the velocity vector. Hence, a 2D intensity profile $\mathbf{I}_0$ translating with velocity $\mathbf{v}_i$ yields the following spatiotemporal image intensity translation:

$$\mathbf{I}(\mathbf{x},t) = \mathbf{I}_0(\mathbf{v}_i(\mathbf{x},t)). \quad (6)$$

We use a negative translational rate in (5) without loss of generality and for mere mathematical convenience.

1.6. Signal Translation in the Frequency Domain

Consider a signal $\mathbf{I}_i(\mathbf{x})$ translating at a constant velocity $\mathbf{v}_i(\mathbf{x},t)$. For this signal, the Fourier transform of the optical flow constraint equation is obtained with the differentiation property as:

$$\mathcal{F}\left[\nabla\mathbf{I}_i(\mathbf{x})^T\mathbf{a}_i + \mathbf{I}_{it}\right] = i\hat{\mathbf{I}}_i(\mathbf{k})\delta(\mathbf{k}^T\mathbf{a}_i + \omega), \quad (7)$$

where i is the imaginary number, $\hat{\mathbf{I}}_i(\mathbf{k})$ is the Fourier transform of $\mathbf{I}_i(\mathbf{x})$ and $\delta(\mathbf{k}^T\mathbf{a}_i + \omega)$ is a Dirac delta function. Expression (7) yields $\mathbf{k}^T\mathbf{a}_i + \omega = 0$ as a constraint on velocity. Similarly, the Fourier transform of a translating image signal $\mathbf{I}_i(\mathbf{x},t)$ is obtained with the shift property as:

$$\begin{aligned}\hat{\mathbf{I}}(\mathbf{k},\omega) &= \int\int \mathbf{I}_i(\mathbf{v}_i(\mathbf{x},t))e^{-i(\mathbf{k}^T\mathbf{x}+\omega t)}d\mathbf{x}dt \\ &= \int\left[\int \mathbf{I}_i(\mathbf{v}_i(\mathbf{x},t))e^{-i\mathbf{k}^T\mathbf{x}}d\mathbf{x}\right]e^{-i\omega t}dt \\ &= \hat{\mathbf{I}}_i(\mathbf{k})\delta(\mathbf{k}^T\mathbf{a}_i + \omega), \quad (8)\end{aligned}$$

which also yields the constraint $\mathbf{k}^T\mathbf{a}_i + \omega = 0$. Hence, (7) and (8) demonstrate that the frequency analysis of image motion is in accordance with the motion constraint equation [18]. It is also observed that $\mathbf{k}^T\mathbf{a}_i + \omega = 0$ represents, in the frequency domain, an oriented plane passing through the origin, with normal vector $\mathbf{a}_i$ descriptive of full velocity, onto which the Fourier spectrum of $\mathbf{I}_i(\mathbf{x})$ lies.

1.7. Related Literature

Traditionally, motion perception has been equated with orientation of power in the frequency domain. The many optical flow methods use what Chubb and Sperling term the Motion-From-Fourier-Components (MFFC) principle [11] in which the orientation of the plane or line through the origin of the frequency space that contains most of the spectral power gives the rate of image translation.

The MFFC principle states that for a moving stimulus, its Fourier transform has substantial power over some regions of the frequency domain whose points spatiotemporally correspond to sinusoidal gratings with drift direction consonant with the perceived motion [11]. In addition, current models of human perception involve some frequency analysis of the imagery, such as band-pass filtering and similar processes. However, some classes of moving stimuli which elicit a strong percept in subjects fail to show a coherent spatiotemporal frequency distribution of their power and cannot be understood in terms of the MFFC principle.

Examples include drift-balanced visual stimuli [11], Fourier and Non-Fourier plaid superpositions [52], amplitude envelopes, sinusoidal beats and various multiplicative phenomena [19]. By drift-balanced it is meant that a visual stimulus with two (leftward and rightward, for example) or more different motions shows identical contents of Fourier power for each motion and therefore, according to the MFFC principle, should not elicit a coherent motion percept. However, some classes of drift-balanced stimuli defined by Chubb and Sperling do elicit strong coherent motion percept-

s, contrary to the predictions of the usual MFFC model.

Sources of Non-Fourier motion also include the motion of texture boundaries and the motion of motion boundaries. For instance, transparency as considered by Fleet and Langley [19] is an example of Non-Fourier motion, as transparency causes the relative scattering of Fourier components away from the spectrum of the moving stimuli. In addition, occlusion, modeled as in (13), is another example of Non-Fourier motion which is closely related to the Theta motion stimuli of Zanker [53], where the occlusion window moves independently from both the foreground and the background, thus involving three independent velocities.

It has been observed by Fleet and Langley that many Non-Fourier motion stimuli have simple characterizations in the frequency domain, namely power distributions located along lines or planes which do not contain the origin of the frequency space, as required by the MFFC idealization [19]. Occlusion and translucency being among those Non-Fourier visual stimuli, we develop their exact frequency representations, state their properties with respect to image motion (or optical flow), consider the aperture problem and include additive translucency phenomena within the theoretical framework.

1.8. Methodology

To analyze the frequency structure of image signals while preserving representations that are as general as possible, an effort is made to only pose those hypotheses that would preserve the generality of the analysis to follow. We describe the assumptions and the proof techniques with which the theoretical results were obtained.

Image Signals The geometry of visual scenes under perspective projection generally yields complex image signals. Conceptually, assumptions concerning scene structure should not be made, as they constrain the geometry of observable scenes. In addition, any measured physical signal, such as image intensities, satisfies Dirichlet conditions. Such signals admit a finite number of finite discontinuities, are absolutely integrable and may be expanded into complex exponential series. Dirichlet conditions constitute the sum of assumptions made on image signals.

Velocity On a local basis, constant models of signal translation may be adequate to describe velocity. However, linear models admit an increased number of deformations, such as signal dilation. Hence, the extent used for signal analysis may be larger with linear models. We considered a constant model of velocity, leaving deformations of higher order for further analysis.

Occluding Boundaries Object frontiers and their projection onto the imaging plane are typically unconstrained in shape and are difficult to model on a large spatial scale. Simpler, local models appear to be more appropriate. The framework includes occlusion boundaries as locally straight edges, represented with step functions. This hypothesis only approximates reality and limits the analysis to local image regions. However, we outline in which way this hypothesis can be relaxed to include occlusion boundaries of any shape.

Proof Techniques The Theorems and their Corollaries established in this analysis emanate from a general approach to modeling visual scenes exhibiting occlusion discontinuities or translucency. An equation which describes the spatio-temporal pattern of the superposition of a background and an occluding signal is established [17], in which a characteristic function describing the position of an occluding signal within the imaging space of the visual sensor is defined:

$$\chi(\mathbf{x}) = \begin{cases} 1 & \text{if } \mathbf{x} \text{ within the occluding signal} \\ 0 & \text{otherwise} \end{cases} \tag{9}$$

and two image signals $\mathbf{I}_1(\mathbf{x})$ and $\mathbf{I}_2(\mathbf{x})$, corresponding to the occluding and occluded signals respectively, are defined to form the overall signal pattern:

$$\begin{aligned} \mathbf{I}(\mathbf{x},t) = & \\ & \chi(\mathbf{v}_1(\mathbf{x},t))\mathbf{I}_1(\mathbf{v}_1(\mathbf{x},t)) + \\ & [1-\chi(\mathbf{v}_1(\mathbf{x},t))]\,\mathbf{I}_2(\mathbf{v}_2(\mathbf{x},t)), \end{aligned} \tag{10}$$

where $\mathbf{v}_i(\mathbf{x},t)$ is constant velocity. Note that the characteristic function describing the object has the same velocity as its corresponding

intensity pattern $\mathbf{I}_1(\mathbf{x})$. In (10) are inserted the hypotheses made on its various components and the structure of occlusion in the frequency domain is developed. That is to say, signal structures are expanded into complex exponential series, such as:

$$\mathbf{I}_i(\mathbf{x}) = \sum_{\mathbf{n}=-\vec{\infty}}^{\vec{\infty}} c_{i\mathbf{n}} e^{i\mathbf{x}^T N \mathbf{k}_i}, \qquad (11)$$

where $\mathbf{I}_i(\mathbf{x})$ is the i^{th} intensity pattern, $c_{i\mathbf{n}}$ are complex coefficients, $\mathbf{k}_i$ are fundamental frequencies, $\mathbf{n}^T = (n_1, n_2, \ldots n_n)$ are integers and $N = \mathbf{n}^T I$. Occlusion boundaries become locally straight edges, represented with step functions such as:

$$\mathbf{U}(\mathbf{x}) = \begin{cases} 1 & \text{if } \mathbf{x}^T \mathbf{n}_1 \geq 0 \\ 0 & \text{otherwise,} \end{cases} \qquad (12)$$

where $\mathbf{n}_1$ is a vector normal to the tangent of the occluding boundary. In addition, degenerate image signals under occlusion are investigated, thus describing the aperture problem in the context of the framework. Whenever technically possible, the theoretical results were compared with numerical experiments using Fast Fourier Transforms operating on synthetically generated image sequences.

Relevance of Fourier Analysis Many algorithms operating in the Fourier domain for which a claim of multiple motions capability is made have been developed [27]. However, this is performed without a complete knowledge of the frequency structure of occlusion phenomena. In addition, Non-Fourier spectra, including occlusion and translucency effects have been conjectured to have mathematically simple characterizations in Fourier space [19]. Consequently, the use of Fourier analysis as a local tool is justified as long as one realizes that it constitutes a global idealization of local phenomena. In that sense, Fourier analysis is used as a local tool whenever Gabor filters, wavelets or local Discrete Fourier Transforms are employed for signal analysis.

Experimental Technique Given the theoretical nature of this contribution, the purpose of the numerical experiments is to verify the validity of the theoretical results. In order to accomplish this, the frequency content of the image signals used in the experiments must be entirely known to the experimenter, thus forbidding the use of natural image sequences. In addition, image signals with single frequency components are used in order to facilitate the interpretation of experiments involving 3D Fast Fourier transforms. The use of more complex signals impedes a careful examination of the numerical results and do not extend the understanding of the phenomena under study in any particular way.

2. Spectral Structure of Occlusion

The analysis begins with the consideration of a simple case of occlusion consisting of two translating sinusoidal signals. These preliminary results are then generalized to arbitrary signals and the aperture problem is examined.

2.1. Sinusoidal Image Signals

The case in which two sinusoidals play the role of the object and the background is first considered. Let $\mathbf{I}_i(\mathbf{x})$ be an image signal translating with velocity $\mathbf{v}_i(\mathbf{x}, t)$ such that $\mathbf{I}_i(\mathbf{x}, t) = \mathbf{I}_i(\mathbf{v}_i(\mathbf{x}, t))$. Its Fourier transform is $\hat{\mathbf{I}}_i(\mathbf{k}, \omega) = \hat{\mathbf{I}}_i(\mathbf{k})\delta(\mathbf{k}^T \mathbf{a}_i + \omega)$. Let $\mathbf{I}_1(\mathbf{x})$ be occluding another image signal $\mathbf{I}_2(\mathbf{x})$, with respective velocities $\mathbf{v}_1(\mathbf{x}, t)$ and $\mathbf{v}_2(\mathbf{x}, t)$. The resulting occlusion scene can then be expressed as:

$$\begin{aligned} &\mathbf{I}(\mathbf{x}, t) = \\ &\quad \mathbf{U}(\mathbf{v}_1(\mathbf{x}, t))\mathbf{I}_1(\mathbf{v}_1(\mathbf{x}, t)) + \\ &\quad (1 - \mathbf{U}(\mathbf{v}_1(\mathbf{v}, t)))\mathbf{I}_2(\mathbf{v}_2(\mathbf{x}, t)), \end{aligned} \qquad (13)$$

where $\mathbf{U}(\mathbf{x})$ is (12). The Fourier transform of (13) is:

$$\begin{aligned} &\hat{\mathbf{I}}(\mathbf{k}, \omega) = \\ &\quad [\hat{\mathbf{U}}(\mathbf{k})\delta(\mathbf{k}^T \mathbf{a}_1 + \omega)] * [\hat{\mathbf{I}}_1(\mathbf{k})\delta(\mathbf{k}^T \mathbf{a}_1 + \omega)] - \\ &\quad [\hat{\mathbf{U}}(\mathbf{k})\delta(\mathbf{k}^T \mathbf{a}_1 + \omega)] * [\hat{\mathbf{I}}_2(\mathbf{k})\delta(\mathbf{k}^T \mathbf{a}_2 + \omega)] + \\ &\quad \hat{\mathbf{I}}_2(\mathbf{k})\delta(\mathbf{k}^T \mathbf{a}_2 + \omega), \end{aligned} \qquad (14)$$

where $\hat{\mathbf{U}}(\mathbf{k})$ is the Fourier transform of a step function $\mathbf{U}(\mathbf{x})$ written as

$$\hat{\mathbf{U}}(\mathbf{k}) = \pi\delta(\mathbf{k}) - \frac{i\delta(\mathbf{k}^T \mathbf{n}_1^{\perp})}{\mathbf{k}^T \mathbf{n}_1}, \qquad (15)$$

THEOREM 1. *Let* $\mathbf{I}_1(\mathbf{x})$ *and* $\mathbf{I}_2(\mathbf{x})$ *be cosine functions with respective angular frequencies* $\mathbf{k}_1^T = 2\pi(f_{1x}, 0)$ *and* $2\pi(0, f_{1y})$, $\mathbf{k}_2^T = 2\pi(f_{2x}, 0)$ *and* $2\pi(0, f_{2y})$ *and let* $\mathbf{I}_1(\mathbf{v}_1(\mathbf{x}, t)) = c_1(\cos(k_{1x}x - a_{13}t) + \cos(k_{1y}y - b_{13}t))$ *and* $\mathbf{I}_2(\mathbf{v}_2(\mathbf{x}, t)) = c_2(\cos(k_{2x}x - a_{23}t) + \cos(k_{2y}y - b_{23}t))$. *The frequency spectrum of the occlusion is:*

$$\begin{aligned}\hat{\mathbf{I}}(\mathbf{k}, \omega) &= \frac{\pi}{4} c_1 \delta(\mathbf{k} \pm \mathbf{k}_1, \omega \mp \mathbf{k}_1^T \mathbf{a}_1) + \frac{(1-\pi)}{4} c_2 \delta(\mathbf{k} \pm \mathbf{k}_2, \omega \mp \mathbf{k}_2^T \mathbf{a}_2) \\ &+ \frac{i c_2 \delta((\mathbf{k} \pm \mathbf{k}_1)^T \mathbf{n}_1^\perp, \mathbf{k}^T \mathbf{a}_1 + \omega \pm \mathbf{k}_2^T \Delta\mathbf{a})}{4(\mathbf{k} \pm \mathbf{k}_2)^T \mathbf{n}_1} - \frac{i c_1 \delta((\mathbf{k} \pm \mathbf{k_1})^T \mathbf{n}_1^\perp, \mathbf{k}^T \mathbf{a}_1 + \omega}{4(\mathbf{k} \pm \mathbf{k}_1)^T \mathbf{n}_1}, \end{aligned} \tag{16}$$

where $\Delta\mathbf{a} = \mathbf{a}_1 - \mathbf{a}_2$ *and* $\mathbf{n}_1$ *is a normal vector perpendicular to the occluding boundary.*

with $\mathbf{n}_1$ as a vector normal to the occlusion boundary and $\mathbf{n}_1^\perp$ as its negative reciprocal $(-n_y, n_x)^T$.

Theorem 1 is derived to examine occlusion with the simplest set of parameters, such as the form of occlusion boundaries, the number of distinct frequencies required to represent both the occluding and occluded image signals, and a constant model of velocity. Even with this constrained domain of derivation, a number of fundamental observations are made, such as: the occlusion in frequency space is formed of the Fourier transform of a step function convolved with every existing frequency of both the occluding and occluded sinusoidal signals and, the power content of the distortion term is entirely imaginary, forming lines of decreasing power which do not contain the origin, around the frequencies of both the occluding and occluded signals. Their orientation is parallel to the spectrum of the occluding signal, and the detection of their orientation allows to identify the occluding velocity, leaving the occluded velocity to be interpreted as such.

We performed a series of experiments to graphically demonstrate the composition of a simple occlusion scene. To simplify the interpretation of the experiments, we used 1D sinusoidal signals composed of single frequencies. In addition, the signals are Gaussian-windowed in order to avoid the Gibbs phenomenon when computing their Fast Fourier Transforms (FFTs). Figure 2a), b) and c) show the components of a simple occlusion scene, pictured in 2d). Figure 2a) is the occluding signal with spatial frequency $\frac{2\pi}{16}$ and velocity -1.0, such that

$$\mathbf{I}_1(x, t) = \cos\left(\frac{2\pi}{16}(x + t)\right) \tag{17}$$

and in 2b) is the occluded signal with spatial frequency $\frac{2\pi}{8}$ and velocity 1.0, yielding

$$\mathbf{I}_2(x, t) = \cos\left(\frac{2\pi}{8}(x - t)\right). \tag{18}$$

The occluding boundary in Figure 2c) is a 1D step function, written as

$$\mathbf{U}(x) = \begin{cases} 1 \text{ if } x \geq 0 \\ 0 \text{ otherwise} \end{cases} \tag{19}$$

and translates with a velocity identical to that of $\mathbf{I}_1$.

The resulting occlusion scene in Figure 2d) is constructed with the following 1D version of (13):

$$\begin{aligned}&\mathbf{I}(x, t) = \\ &\quad \mathbf{I}_1(v_1(x, t))\chi(v_1(x, t)) + \\ &\quad [1 - \chi(v_1(x, t))]\, \mathbf{I}_2(v_2(x, t)),\end{aligned} \tag{20}$$

where $\mathbf{I}_1$ is (17), $\mathbf{I}_2$ is (18) and χ is (19). Figures 2e) through h) show the amplitude spectra of figures 2a) through d) respectively, where it is easily observed the the spectrum of the step function (19) is convolved with each frequency of both sinusoidals. Further, Theorem 1 predicts Fourier spectra such as 2h) in their entirety as is demonstrated by the experiments in section 2.3.

2.2. Generalized Image Signals

For this analysis to gain generality, we need to find a suitable set of mathematical functions to represent physical quantities such as image signals that lend themselves to the analysis to follow and which do not impose unnecessary hypotheses on the structure of those signals.

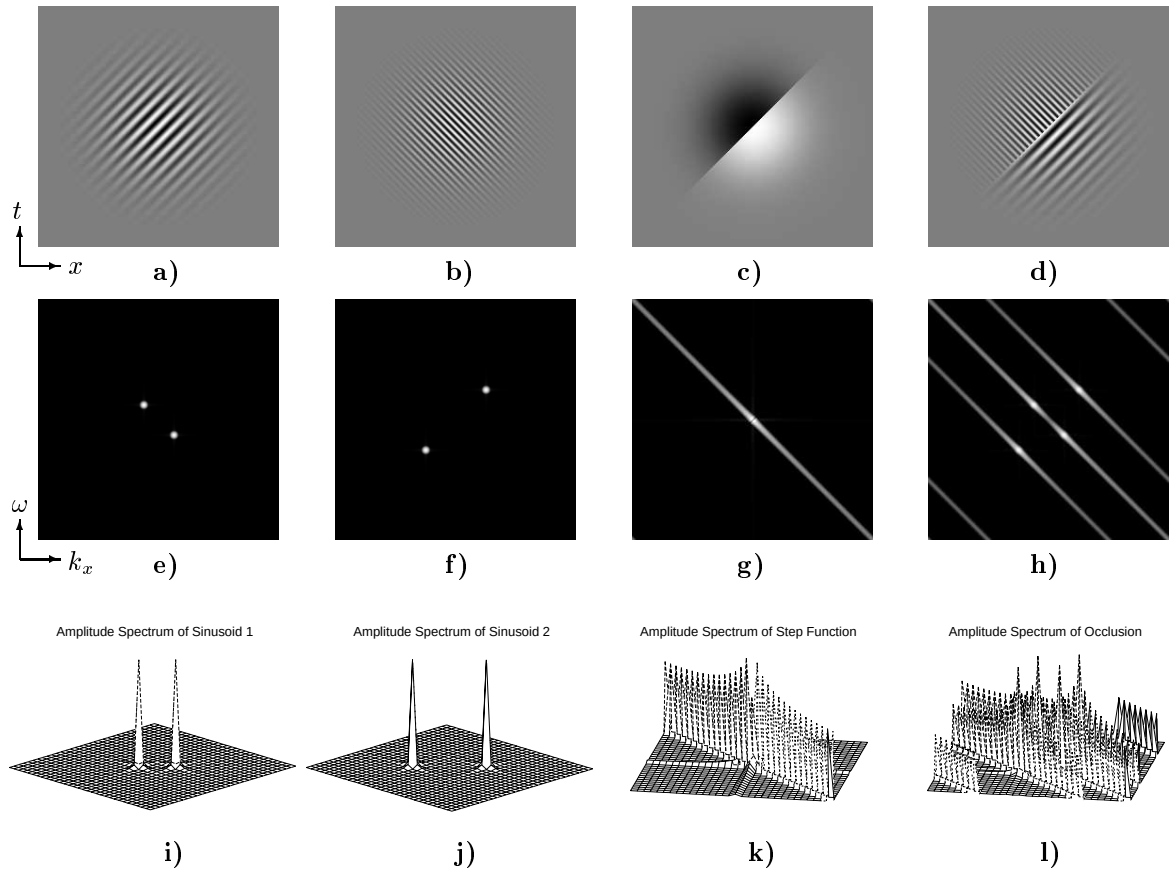

Fig. 2. **(top):** *The composition of a simple 1D occlusion scene.* **a)** *The occluding sinusoidal signal with frequency* $\frac{2\pi}{16}$ *and velocity* -1.0. **b)** *The occluded sinusoidal signal with frequency* $\frac{2\pi}{8}$ *and velocity* 1.0. **c)** *The translating step function used to create the occlusion scene.* **d)** *The occlusion as a combination of* **a)**, **b)** *and* **c)**. **(center):** *Image plots of amplitude spectra and* **(bottom):** *amplitude spectra as 3D graphs.*

For this purpose we hypothesize that image signals satisfy Dirichlet conditions in the sense that for any interval $x_1 \leq x \leq x_2$, the function $f(x)$ representing the signal must be single-valued, have a finite number of maxima and minima and a finite number of finite discontinuities. Finally, $f(x)$ should be absolutely integrable in such a way that, within the interval, we obtain

$$\int_{x_1}^{x_2} |f(x)|dx < \infty. \tag{21}$$

In addition, any function representing a physical quantity satisfies Dirichlet conditions. Hence, those conditions can be assumed for visual signals without loss of generality and, in this context, the complex exponential series expansion, or Fourier series

$$\sum_{n=-\infty}^{\infty} c_n e^{ink_0 x} \tag{22}$$

converges uniformly to $f(x)$.

Theorem 2 generalizes Theorem 1 from sinusoidal to arbitrary signals. Theorems 1 and 2 introduce the approximation of occluding boundaries with step functions and, as surfaces of any shape may be imaged, the forms of their boundaries are typically unconstrained. On a local basis, however, as long as the spatial extent of analy-

THEOREM 2. *Let $\mathbf{I}_1(\mathbf{x})$ and $\mathbf{I}_2(\mathbf{x})$ be 2D functions satisfying Dirichlet conditions such that they may be expressed as complex exponential series expansions:*

$$\mathbf{I}_1(\mathbf{x}) = \sum_{\mathbf{n}=-\vec{\infty}}^{\vec{\infty}} c_{1\mathbf{n}} e^{i\mathbf{x}^T N\mathbf{k}_1} \quad \textit{and} \quad \mathbf{I}_2(\mathbf{x}) = \sum_{\mathbf{n}=-\vec{\infty}}^{\vec{\infty}} c_{2\mathbf{n}} e^{i\mathbf{x}^T N\mathbf{k}_2}, \tag{23}$$

where $\mathbf{n} = (n_x, n_y)^T$ and $N = \mathbf{n}^T I$ are integers, $\mathbf{x}$ are spatial coordinates, $\mathbf{k}_1 = (k_{1x}, k_{1y})^T$ and $\mathbf{k}_2 = (k_{2x}, k_{2y})^T$ are fundamental frequencies and $c_{1\mathbf{n}}$ and $c_{2\mathbf{n}}$ are complex coefficients. Let $\mathbf{I}_1(\mathbf{x}, t) = \mathbf{I}_1(\mathbf{v}_1(\mathbf{x}, t))$, $\mathbf{I}_2(\mathbf{x}, t) = \mathbf{I}_2(\mathbf{v}_2(\mathbf{x}, t))$ and the occluding boundary be represented by:

$$\mathbf{U}(\mathbf{x}) = \begin{cases} 1 & \textit{if } \mathbf{x}^T\mathbf{n}_1 \geq 0 \\ 0 & \textit{otherwise,} \end{cases} \tag{24}$$

where $\mathbf{n}_1$ is a vector normal to the occluding boundary. The frequency spectrum of the occlusion is:

$$\begin{aligned} \hat{\mathbf{I}}(\mathbf{k}, \omega) \;=\; & \pi \sum_{\mathbf{n}=-\vec{\infty}}^{\vec{\infty}} c_{1\mathbf{n}} \delta(\mathbf{k} - N\mathbf{k}_1, \omega + \mathbf{a}_1^T N\mathbf{k}_1) + (1-\pi) \sum_{\mathbf{n}=-\vec{\infty}}^{\vec{\infty}} c_{2\mathbf{n}} \delta(\mathbf{k} - N\mathbf{k}_2, \omega + \mathbf{a}_2^T N\mathbf{k}_2) - \\ & - i \sum_{\mathbf{n}=-\vec{\infty}}^{\vec{\infty},} \left(\frac{c_{1\mathbf{n}} \delta((\mathbf{k} - N\mathbf{k}_1)^T \mathbf{n}_1^\perp, \mathbf{k}^T\mathbf{a}_1 + \omega)}{(\mathbf{k} - N\mathbf{k}_1)^T \mathbf{n}_1} + \frac{c_{2\mathbf{n}} \delta((\mathbf{k} - N\mathbf{k}_2)^T \mathbf{n}_1^\perp, \mathbf{k}^T\mathbf{a}_1 + \omega - \Delta\mathbf{a}^T N\mathbf{k}_2)}{(\mathbf{k} - N\mathbf{k}_2)^T \mathbf{n}_1} \right), \end{aligned} \tag{25}$$

where $\Delta\mathbf{a} = \mathbf{a}_1 - \mathbf{a}_2$.

sis remains sufficiently small, the approximation of occluding boundaries as straight-edged lines is sufficient and greatly simplifies the derivation of the results. Also for simplicity, a constant model of velocity is adopted, which is thought of as a valid local approximation of reality [4, 32]. However, the constraint on the shape of the occluding boundary may be removed while preserving the validity of most of the theoretical results, as we later demonstrate. As expected, the sum of properties identified in Theorem 1 hold for Theorem 2. For instance, it is found that the Fourier spectrum of the occluding boundary is convolved with every existing frequency of both the occluding and occluded signals in a manner consonant with its velocity. That is to say, its spectral orientation is descriptive of the motion of the occluding signal. Hence we state the following corollary:

COROLLARY 1. *Under an occlusion phenomenon, the velocities of the occluding and occluded signals can always be identified as such.*

Under occlusion, the spectral orientation of the occluding boundary is parallel to the plane descriptive of the occluding velocity and detecting the spectral orientation of the boundary amounts to identify the occluding velocity, leaving the occluded velocity to be considered as such.

Figure 3 demonstrates the composition of a simple 2D occlusion scene and the Fourier spectra of its components. Figure 3a) is the occluding signal with spatial frequency $(\frac{2\pi}{16}, \frac{2\pi}{16})$ and velocity $(-1.0, -1.0)$ such that

$$\mathbf{I}_1(\mathbf{x}, t) = \cos\left(\frac{2\pi}{16}(x+t)\right) + \cos\left(\frac{2\pi}{16}(y+t)\right)$$

and Figure 3b) is the occluded signal with spatial frequency $(\frac{2\pi}{8}, \frac{2\pi}{8})$ and velocity $(1.0, 1.0)$, yielding

$$\mathbf{I}_2(\mathbf{x}, t) = \cos\left(\frac{2\pi}{8}(x-t)\right) + \cos\left(\frac{2\pi}{8}(y-t)\right).$$

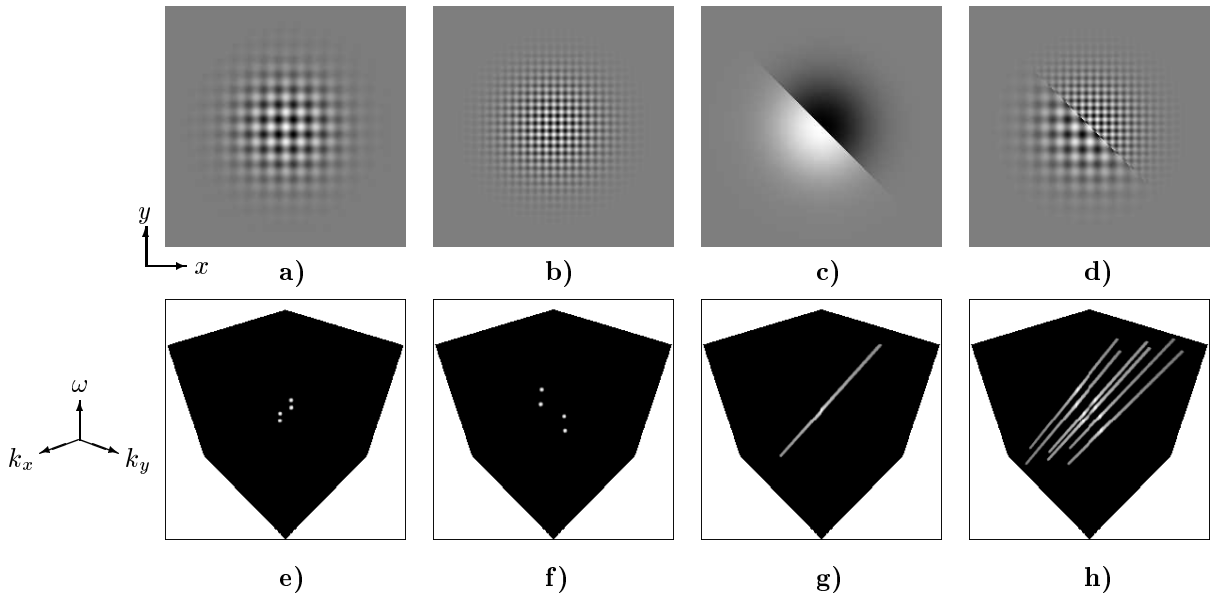

Fig. 3. **(top):** *The composition of a simple 2D occlusion scene.* **a)** *The occluding sinusoidal signal with frequency* $(\frac{2\pi}{16}, \frac{2\pi}{16})$ *and velocity* $(-1.0, -1.0)$. **b)** *The occluded sinusoidal signal with frequency* $(\frac{2\pi}{8}, \frac{2\pi}{8})$ *and velocity* $(1.0, 1.0)$. **c)** *The step function used to create the occlusion scene with normal vector* $(\frac{\sqrt{2}}{2}, \frac{\sqrt{2}}{2})$. **d)** *The occlusion as a combination of* **a)**, **b)** *and* **c)**. **(bottom) e)** *through* **h):** *Image plots of corresponding amplitude spectra.*

The occluding boundary in Figure 3c) is a 2D step function identical to (12) and translates with a velocity which equals that of $\mathbf{I}_1$, the occluding signal. The resulting occlusion scene in Figure 3d) is constructed with (13). Figures 3e) through h) show the 3D amplitude spectra of Figures 3a) through d), respectively.

In the experiments with 2D signals depicted in Figure 4, the spatial frequencies of the occluding and occluded signals are $\mathbf{k}_1^T = (\frac{2\pi}{16}, \frac{2\pi}{16})$ and $\mathbf{k}_2^T = (\frac{2\pi}{8}, \frac{2\pi}{8})$ respectively. Only the velocities and the orientation of the occlusion boundary vary. The velocities of the occluding and occluded signals and the occlusion boundary normal vectors, from left to right in Figure 3, are **a)** $\mathbf{a}_1^T = (-1.0, -1.0)$, $\mathbf{a}_2^T = (1.0, 1.0)$ and $\mathbf{n}_1^T = (\frac{\sqrt{2}}{2}, \frac{\sqrt{2}}{2})$; **b)** $\mathbf{a}_1^T = (1.0, 1.0)$, $\mathbf{a}_2^T = (-1.0, -1.0)$ and $\mathbf{n}_1^T = (\frac{\sqrt{2}}{2}, \frac{\sqrt{2}}{2})$; **c)** $\mathbf{a}_1^T = (-1, -1)$, $\mathbf{a}_2^T = (1, 1)$ and $\mathbf{n}_1^T = (1.0, 0)$, respectively.

As per Theorem 1, the spectral extrema located at $\pm(\mathbf{k}_1, -\mathbf{k}_1^T\mathbf{a}_1)$ and $\pm(\mathbf{k}_2, -\mathbf{k}_2^T\mathbf{a}_2)$ depict the spatiotemporal frequencies of both signals and fit the constraint planes $\mathbf{k}^T\mathbf{a}_1 + \omega = 0$ and $\mathbf{k}^T\mathbf{a}_2 + \omega = 0$. The oblique spectra intersecting the peaks are the convolutions of the spectrum of the step function with the frequencies of both signals and fit lines described by the intersection of planes $(\mathbf{k} \pm \mathbf{k}_1)^T\mathbf{n}_1^\perp = 0$ and $\mathbf{k}_1^T\mathbf{a}_1 + \omega \pm \mathbf{k}_2^T\mathbf{a}_2 = 0$. These spectra are parallel to the constraint plane of the occluding signal and are consonant with its velocity.

Theorem 2 is the generalization of Theorem 1 from sinusoidal to arbitrary signals and its geometric interpretation is similar. For instance, frequencies $(N\mathbf{k}_1, -\mathbf{a}_1^T N\mathbf{k}_1)$ and $(N\mathbf{k}_2, -\mathbf{a}_2^T N\mathbf{k}_2)$ fit the constraint planes of the occluding and occluded signals, defined as $\mathbf{k}^T\mathbf{a}_1 + \omega = 0$ and $\mathbf{k}^T\mathbf{a}_2 + \omega = 0$. In the distortion term, the Dirac δ function with arguments $(\mathbf{k} - N\mathbf{k}_2)^T\mathbf{n}_1^\perp$ and $\mathbf{k}^T\mathbf{a}_1 + \omega - \Delta\mathbf{a}^T N\mathbf{k}_2$ represent a set of lines parallel to the constraint plane of the occluding signal $\mathbf{k}^T\mathbf{a}_1 + \omega = 0$ and, for every discrete frequency $N\mathbf{k}_1$ and $N\mathbf{k}_2$ exhibited by both signals, there is a frequency spectrum fitting the lines given by the intersection of planes $\mathbf{k}^T\mathbf{a}_1 + \omega - \Delta\mathbf{a}^T N\mathbf{k}_2 = 0$

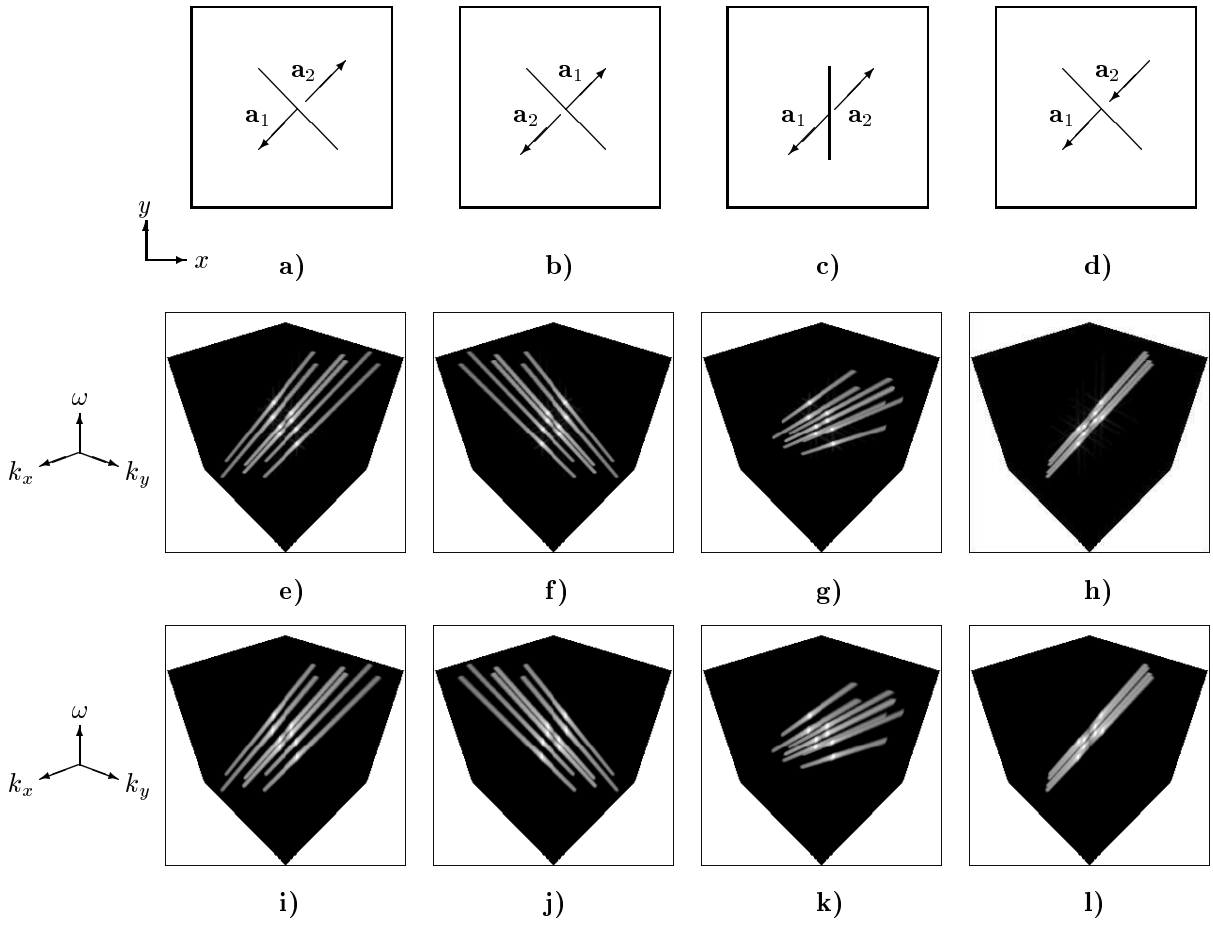

Fig. 4. Four cases of predicted and computed Fourier spectra of occlusion scenes. In all cases the frequencies of the occluding and the occluded signals are $(\frac{2\pi}{16}, \frac{2\pi}{16})$ *and* $(\frac{2\pi}{8}, \frac{2\pi}{8})$. **(top): a)** *Occluding and occluded velocities* $\mathbf{a}_1 = (-1.0, -1.0)$ *and* $\mathbf{a}_2 = (1.0, 1.0)$. **b)** *Occluding and occluded velocities* $\mathbf{a}_1 = (1.0, 1.0)$ *and* $\mathbf{a}_2 = (-1.0, -1.0)$. **c)** *Occluding and occluded velocities* $\mathbf{a}_1 = (-1.0, -1.0)$ *and* $\mathbf{a}_2 = (1.0, 1.0)$ *and boundary normal* $(1.0, 0)$. **d)** *Occluding and occluded velocities* $\mathbf{a}_1 = \mathbf{a}_2 = (-1.0, -1.0)$. **(center) e)** *through* **h):** *Computed FFTs of corresponding occlusion scenes.* **(bottom) i)** *through* **l):** *Fourier spectra predicted by theoretical results.*

and $(\mathbf{k} - N\mathbf{k}_1)^T \mathbf{n}_1^{\perp} = 0$. The magnitudes of these spectra are determined by their corresponding scaling functions $c_{1\mathbf{n}}[(\mathbf{k} - N\mathbf{k}_1)^T \mathbf{n}_1\ ]^{-1}$ and $c_{2\mathbf{n}}[(\mathbf{k} - N\mathbf{k}_2)^T \mathbf{n}_1\ ]^{-1}$. Theorem 2 reveals useful constraint planes, as the power spectra of both signals peak within planes $\mathbf{k}^T\mathbf{a}_1 + \omega = 0$ and $\mathbf{k}^T\mathbf{a}_2 + \omega = 0$ and the constraint planes arising from the distortion are parallel to the spectrum of the occluding signal $\mathbf{I}_1(\mathbf{x}, t)$.

3. The Aperture Problem: Degenerate Cases

In the Fourier domain, the power spectrum of a degenerate signal is concentrated along a linear rather than a planar structure. To see this, consider a 1D signal moving with a constant model of velocity in a 2D space, in the direction of the gradient normal $\mathbf{n}_i$ and with speed s_i:

$$\mathbf{I}(\mathbf{x}, t) = \mathbf{I}_i(\mathbf{x}^T\mathbf{n}_i - s_i t) \tag{26}$$

The Fourier transform of this signal is given by

$$\hat{\mathbf{I}}(\mathbf{k},\omega) = \hat{\mathbf{I}}_i \left(\mathbf{k}^T\mathbf{n}_i\right) \delta\left(\mathbf{k}^T\mathbf{n}_i^{\perp}\right) \delta\left(s_i\mathbf{k}^T\mathbf{n}_i + \omega\right), \tag{27}$$

where $\mathbf{n}_i^{\perp}$ is the negative reciprocal of $\mathbf{n}_i$. The Dirac delta functions represent planar spectra and their intersection forms a linear constraint onto which the spectrum of the degenerate signal resides. Therefore, the planar orientation describing full velocity is undetermined. However, the presence of an occlusion boundary disambiguates the measurement of a degenerate occluding signal in most cases as a straight-edged occlusion boundary provides one constraint on normal velocity and so does its corresponding degenerate occluding signal. Since these structures have an identical full velocity, these constraints should be consistent with it, allowing to form a system of equations to obtain full velocity. For instance, consider the Fourier transform of a translating occluding degenerate signal expressed as its complex exponential series expansion:

$$\int \mathbf{I}_1(\mathbf{x}^T\mathbf{n}_1 - s_1 t) e^{-i(\mathbf{k}^T\mathbf{x}+\omega t)} d\mathbf{x} = \sum_{n=-\infty}^{\infty} c_{in}\delta(\mathbf{k} - nk_1\mathbf{n}_1, \omega + s_1 nk_1), \tag{28}$$

where $\mathbf{n}_1$ is the normal of the signal, s_1 is its speed and $k_1 = \mathbf{k}^T\mathbf{n}_1$ is the fundamental frequency. Additionally, consider the Fourier transform of the occluding boundary with normal vector $\mathbf{n}_2$ and speed s_2:

$$\pi\delta(\mathbf{k},\omega) - \frac{i\delta(\mathbf{k}^T\mathbf{n}_2^{\perp})\delta(s_2\mathbf{k}^T\mathbf{n}_2 + \omega)}{\mathbf{k}^T\mathbf{n}_2}. \tag{29}$$

The convolution of (4) and (29) yields the following spectrum:

$$\begin{aligned} &\pi \sum_{n=-\infty}^{\infty} c_{1n}\delta(\mathbf{k} - nk_1\mathbf{n}_1, \omega + s_1 nk_1) \\ &- i\sum_{n=-\infty}^{\infty} \left(c_{1n} \frac{\delta(\mathbf{k}^T\mathbf{n}_2^{\perp} - nk_1\mathbf{n}_1^T\mathbf{n}_2^{\perp})}{(\mathbf{k} - nk_1\mathbf{n}_1)^T\mathbf{n}_2} \times \right. \\ &\left. \frac{\delta(s_1\mathbf{k}^T\mathbf{n}_2 + \omega + nk_1(s_1 - s_2\mathbf{n}_1^T\mathbf{n}_2))}{(\mathbf{k} - nk_1\mathbf{n}_1)^T\mathbf{n}_2} \right). \end{aligned} \tag{30}$$

Expression (30) allows to derive two directional vectors, fitting the spectra of the degenerate occluding signal and boundary respectively, which are $\mathbf{d}_1^T = (\mathbf{n}_1^T, -s_1)$ and $\mathbf{d}_2^T = (\mathbf{n}_2^T, -s_2)$. Their cross product yields a vector $\mathbf{a}_1$ normal to the planar structure containing both spectra, which is the full velocity of the degenerate occluding signal. The constraints on normal velocities form the following system of equations

$$\begin{aligned} \mathbf{a}_1^T\mathbf{n}_1 - s_1 &= 0 \\ \mathbf{a}_1^T\mathbf{n}_2 - s_2 &= 0 \end{aligned} \tag{31}$$

and its solution, obtained by dividing $\mathbf{d}_1 \times \mathbf{d}_2$ with its third component, is

$$\mathbf{a}_1 = \frac{1}{\mathbf{n}_1^T\mathbf{n}_2^{\perp}} \left(s_1\mathbf{n}_2^{\perp} - s_2\mathbf{n}_1^{\perp}\right), \tag{32}$$

which is full velocity when a constant model is used. This system has a unique solution if and only if $\mathbf{n}_1 \neq \mathbf{n}_2$. Otherwise, if $\mathbf{n}_1 = \mathbf{n}_2$ then $s_1 = s_2$ and (31) has no unique solution. Thus, we state the following Theorem:

THEOREM 3. *The full velocity of a degenerate occluding signal is obtainable from the structure of the Fourier spectrum if and only if its normal is different from the normal of the occlusion boundary.*

We performed experiments with degenerate signals as shown in Figure 5. An occluding degenerate sinusoidal pattern with spatial orientation $\mathbf{n}_1 = (-1.0, 1.0)$ and translating with normal velocity $s1 = 1.0$ is depicted in Figure 5a). The pattern was generated according to

$$\mathbf{I}_1(\mathbf{x}, t) = \cos\left(\frac{2\pi}{16}(\mathbf{x}^T\mathbf{n}_1 - s_1 t)\right). \tag{33}$$

As can be seen from its Fourier transform 5e), the frequency content is composed of two δ functions from which only a normal velocity estimate can be obtained by computing the orientation of the line passing through the spectral peaks and the origin of the frequency space.

Figure 5b) shows the occluding signal and the occlusion edge combination. The normal vector to the edge is $\mathbf{n} = (1.0, 1.0)$. The Fourier transform is shown in 5f), where the spectrum of the edge is convolved with the peaks of the signal. In this case, the full velocity of the degenerate signal is obtained by computing the normal vector to the plane containing the entire spectrum

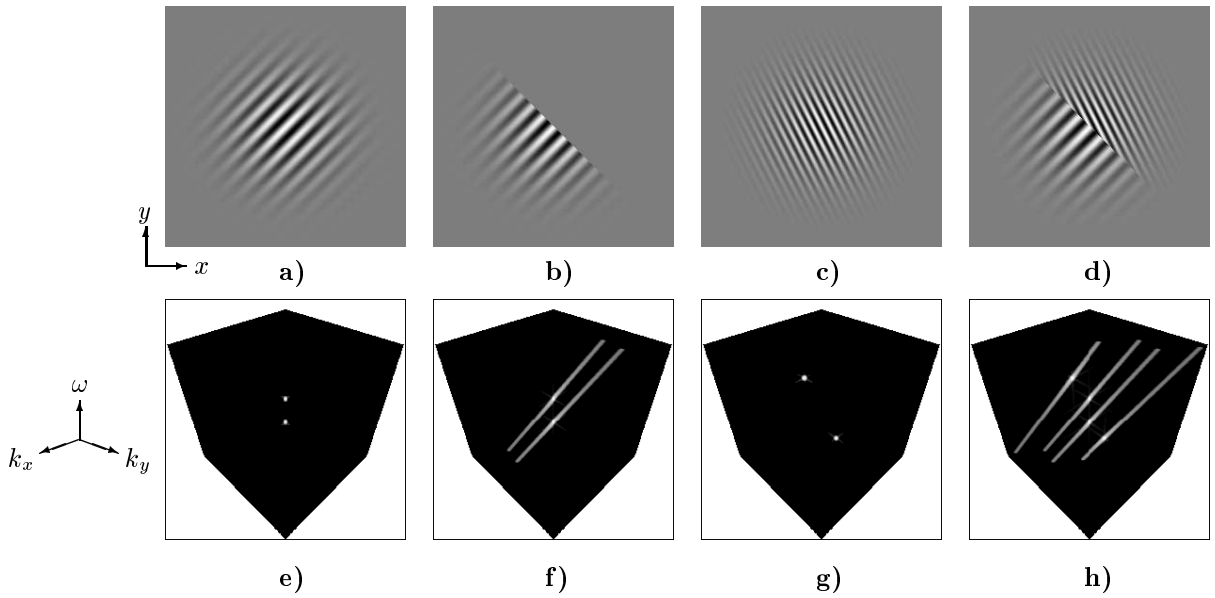

Fig. 5. Cases of degenerate occluding signals. **(top): a)** *Occluding signal with normal* $\mathbf{n}_1 = (-1.0, 1.0)$. **b)** *Occluding signal and boundary with normal* $\mathbf{n} = (1.0, 1.0)$. **c)** *Occluded signal with normal* $\mathbf{n}_2 = (2.0, 1.0)$. **d)** *Complete occlusion scene.* **(bottom) e)** *through* **h):** *Corresponding frequency spectra.*

and the origin of the frequency space. Figure 5c) shows the occluded signal with spatial orientation $\mathbf{n}_2 = (2.0, 1.0)$ and translating with normal velocity $s_2 = 2.0$. This pattern was generated according to

$$\mathbf{I}_2(\mathbf{x}, t) = \cos\left(\frac{2\pi}{8}(\mathbf{x}^T\mathbf{n}_2 - s_2 t)\right) \qquad (34)$$

and its frequency content appears in 5g).

The complete occlusion scene is shown in 5d) and the corresponding frequency content is depicted in 5h). To disambiguate the normal velocity of the occluding signal, it is first necessary to identify the occluding velocity. This is accomplished by finding a line that is parallel to the spectral orientation of the Fourier transform of the occluding edge and that also contains the frequency content of one signal. In this case, this signal is said to be occluding, and the normal to the plane containing its frequency spectrum, including the spectrum of the occluding edge convolved with its discrete frequencies, yields a full velocity measurement.

4. Related Considerations

In this section we consider the relationship between additive translucency and the theoretical framework, the effects of occluding edges away from the origin of the spatiotemporal domain, occluding boundaries of various shapes and the relevancy of the theoretical model with respect to Non-Fourier motions such as Zanker's Theta motions [53].

4.1. Translucency

Transmission of light through translucent material may cause multiple motions to arise within an image region. Generally, this effect is depicted on the image plane as

$$\mathbf{I}(\mathbf{x}, t) = f(\rho_1)(\mathbf{v}_1(\mathbf{x}, t))\mathbf{I}_2(\mathbf{v}_2(\mathbf{x}, t)), \qquad (35)$$

where $f(\rho_1)$ is a function of the density of the translucent material [17]. Under the local assumption of spatially constant $f(\rho_1)$ with translucency factor φ, (35) is reformulated as a weighted super-

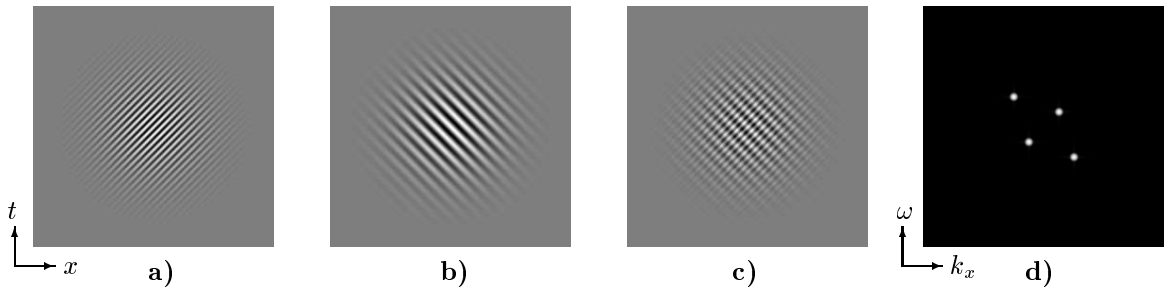

Fig. 6. The composition of an additive transparency scene. **a):** *First sinusoidal signal with frequency* $k_1 = \frac{2\pi}{8}$ *and velocity* $a_1 = 1.0$. **b):** *Second sinusoidal signal with frequency* $k_2 = \frac{2\pi}{16}$ *and velocity* $a_2 = -1.0$. **c):** *Transparency created with the superposition of first and second sinusoidal signal.* **d):** *Frequency spectrum of transparency.*

position of intensity profiles, written as

$$\mathbf{I}(\mathbf{x},t) = \varphi \mathbf{I}_1(\mathbf{v}_1(\mathbf{x},t)) + (1-\varphi)\mathbf{I}_2(\mathbf{v}_2(\mathbf{x},t)), \quad (36)$$

where $\mathbf{I}_1(\mathbf{v}_1(\mathbf{x},t))$ is the intensity profile of the translucent material and $\mathbf{I}_2(\mathbf{v}_2(\mathbf{x},t))$ is the intensity profile of the background. With $\mathbf{I}_1(\mathbf{v}_1(\mathbf{x},t))$ and $\mathbf{I}_2(\mathbf{v}_2(\mathbf{x},t))$ satisfying Dirichlet conditions, the frequency spectrum of (36) is written as:

$$\begin{aligned}\hat{\mathbf{I}}(\mathbf{k},\omega) = \\ \varphi \sum_{\mathbf{n}=-\vec{\infty}}^{\vec{\infty}} c_{1\mathbf{n}}\delta(\mathbf{k} - N\mathbf{k}_1, \omega + \mathbf{a}_1^T N\mathbf{k}_1) + \\ (1-\varphi)\sum_{\mathbf{n}=-\vec{\infty}}^{\vec{\infty}} c_{2\mathbf{n}}\delta(\mathbf{k} - N\mathbf{k}_2, \omega + \mathbf{a}_2^T N\mathbf{k}_2).\end{aligned} \quad (37)$$

Hence, with respect to its frequency structure, translucency may be reduced to a special case of occlusion for which the distortion terms vanish. Figure 6 shows the Fourier transform of an additive translucency composed of two sinusoidals.

4.2. Phase Shifts

For reasons of simplicity and clarity, in each Theorem and numerical result, the occluding boundary contained the origin of the coordinate system. We generalize this by describing the occlusion boundary as

$$\mathbf{U}(\mathbf{x}) = \begin{cases} 1 \text{ if } \mathbf{x}^T\mathbf{n} + y_0 \geq 0 \\ 0 \text{ otherwise} \end{cases}, \quad (38)$$

where y_0 is the y-axis intercept. The Fourier spectrum of such a boundary includes a phase shift and is written as:

$$e^{iy_0\mathbf{k}^T\mathbf{n}_i}\left[\pi\delta(\mathbf{k}) - \frac{i\delta(\mathbf{k}^T\mathbf{n}_i^{\perp})}{\mathbf{k}^T\mathbf{n}_i}\right]\delta(\mathbf{k}^T\mathbf{a}_i + \omega) \quad (39)$$

Equation (39) can be further simplified as:

$$\pi\delta(\mathbf{k}) - \frac{ie^{iy_0\mathbf{k}^T\mathbf{n}_i}\delta(\mathbf{k}^T\mathbf{n}_i^{\perp}, \mathbf{k}^T\mathbf{a}_i + \omega)}{\mathbf{k}^T\mathbf{n}_i} \quad (40)$$

The Fourier spectrum of the boundary is to be convolved with the complex exponential series expansions of the occluding and occluded signals and subsequently with the Fourier transform of the Gaussian window. In the case of the occluding signal, the convolution with the the shifted occlusion boundary can be written as:

$$\begin{aligned}\pi \sum_{\mathbf{n}=-\vec{\infty}}^{\vec{\infty}} c_{1\mathbf{n}}\delta(\mathbf{k} - N\mathbf{k}_1, \omega + \mathbf{a}_1^T N\mathbf{k}_1) - \\ ie^{iy_0(\mathbf{k}-N\mathbf{k}_1)^T\mathbf{n}_1}\frac{c_{1\mathbf{n}}\delta((\mathbf{k}-N\mathbf{k}_1)^T\mathbf{n}_1^{\perp}, \omega + \mathbf{k}^T\mathbf{a}_1)}{(\mathbf{k}-N\mathbf{k}_1)^T\mathbf{n}_1}\end{aligned} \quad (41)$$

and, similarly for the occluded signal:

$$\begin{aligned}\pi \sum_{\mathbf{n}=-\vec{\infty}}^{\vec{\infty}} c_{2\mathbf{n}}\delta(\mathbf{k} - N\mathbf{k}_2, \omega + \mathbf{a}_2^T N\mathbf{k}_2) - \\ ie^{iy_0(\mathbf{k}-N\mathbf{k}_2)^T\mathbf{n}_1}\frac{c_{2\mathbf{n}}\delta((\mathbf{k}-N\mathbf{k}_2)^T\mathbf{n}_1^{\perp}, \omega + \mathbf{k}^T\mathbf{a}_2)}{(\mathbf{k}-N\mathbf{k}_2)^T\mathbf{n}_1}\end{aligned} \quad (42)$$

These convolutions are combined together as before to obtain the Fourier spectrum of occlusion

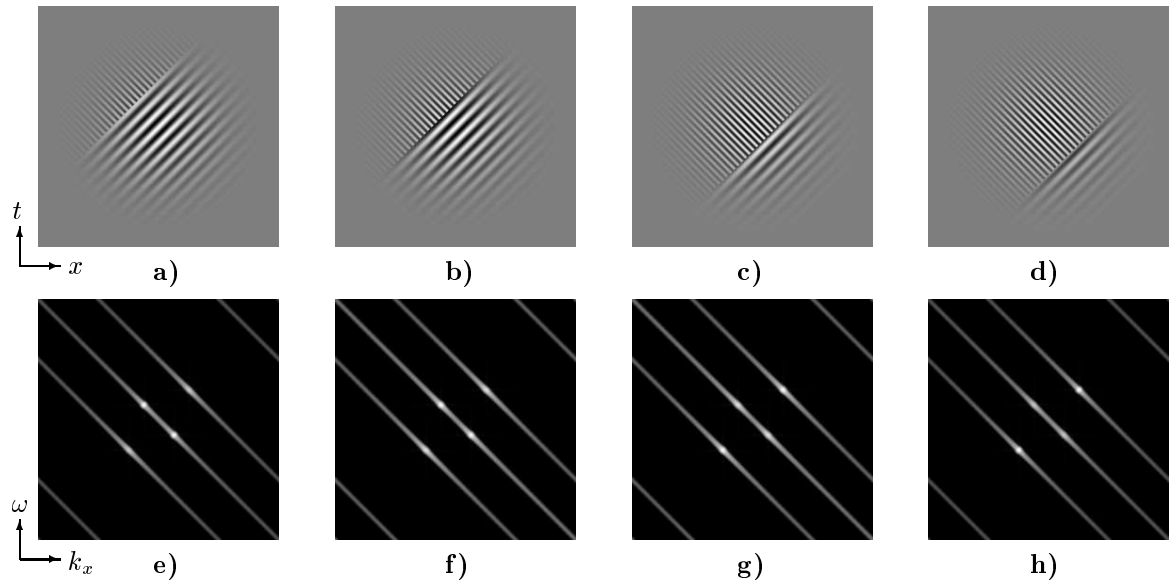

Fig. 7. Phase shifts from occluding edge. **(top): a)** $y_0 = -20.0$. **b)** $y_0 = -10.0$. **c)** $y_0 = 10.0$. **d)** $y_0 = 20.0$. **(bottom) e)** *through* **h):** *Corresponding frequency spectra. The relative magnitude between the occluding and occluded signals depend on their respective visible areas under the Gaussian envelope. For instance, The frequencies of the occluding signal dominate over those of the occluded signal in* **e)**, *and vice versa in* **h)**.

with an occluding boundary not containing the origin of the space.

We conducted experiments with 1D image signals and shifted the occlusion point with different values of y_0 in (38). As observed in Figure 7, these phase shifts do not alter the structure of occlusion in frequency space. The variations in the amplitude spectra are due to the Gaussian windowing of the occlusion scene. For instance, the frequency peaks of the occluding signal in Figure 7e) show more power than those of the occluded signal, owing to the fact that the signal is dominant within the Gaussian window. The contrary is observed when the occluded signal occupies most of the window, as shown in Figure 7h).

4.3. Generalized Occluding Boundaries

Typically, occlusion boundaries are unconstrained in shape, yielding a variety of occluding situations. Under the hypothesis that the motion of the occluding boundary is rigid on the image plane, we can derive the frequency structure of such occlusion events. For instance, consider a generalized occlusion boundary represented by the characteristic function $\chi(\mathbf{x})$ in the coordinates of the image plane and the Fourier transforms of the complex exponential series expansions of both the occluding and occluded signals $\mathbf{I}_1$ and $\mathbf{I}_2$. Substituting these terms into (13) yields the following Fourier spectrum

$$\begin{aligned}\hat{\mathbf{I}}(\mathbf{k},\omega) = & \\ & \sum_{\mathbf{n}=-\vec{\infty}}^{\vec{\infty}} c_{1\mathbf{n}}\hat{\chi}(\mathbf{k}-N\mathbf{k}_1)\delta(\mathbf{a}_1^T\mathbf{k}+\omega) - \\ & \sum_{\mathbf{n}=-\vec{\infty}}^{\vec{\infty}} c_{2\mathbf{n}}\hat{\chi}(\mathbf{k}-N\mathbf{k}_2)\delta(\mathbf{a}_2^T\mathbf{k}+\omega-\Delta\mathbf{a}^T N\mathbf{k}_2) \\ + & \sum_{\mathbf{n}=-\vec{\infty}}^{\vec{\infty}} c_{2\mathbf{n}}\delta(\mathbf{k}-N\mathbf{k}_2,\omega+\mathbf{a}_2^T N\mathbf{k}_2) \end{aligned} \tag{43}$$

from which it is easily observed that the spectrum of the occluding boundary is repeated at every non-zero frequency of both signals. The spectrum

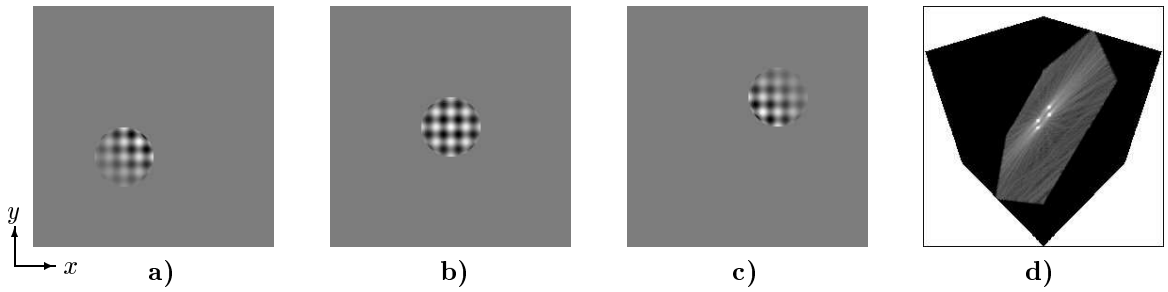

Fig. 8. Generalized occluding boundaries. **a), b)** *and* **c):** *Images from a sequence in which the occluding pattern moves with velocity* $\mathbf{a}_1^T = (-1.0, -1.0)$. *Spatial frequency of the sinusoidal texture within the circular boundary is* $\mathbf{k}_1^T = (\frac{2\pi}{16}, \frac{2\pi}{16})$. **d):** *The frequency spectrum of the sequence, where the plane contains the spectrum of the boundary convolved with the frequency of the texture.*

occupies a plane descriptive of full velocity and can be used to perform such measurements.

Figure 8 shows an experiment where the occluding signal is within a circular occlusion boundary. The signal and boundary are moving at a constant velocity $\mathbf{a}_1^T = (-1.0, -1.0)$ and the occluded signal is a background of constant intensity. Figures 8a) through c) show the motion of the occluding region while Figure 8d) is the frequency spectrum of the sequence, from which we observe the spectrum of the circular boundary and the peaks representing the frequencies of the occluding sinusoidal texture are confined to a planar region fully descriptive of the image motion.

4.4. Non-Fourier Motion

Non-Fourier motion is characterized by its inability to be explained by the MFFC principle. In other terms, such motions generate power distributions that are inconsistent with translational motion. Sources of Non-Fourier motion include such phenomena as translucency and occlusion and, in particular, Zanker's Theta motion stimuli involving occlusion [53]. This category of motion is described by an occlusion window that translates with a velocity that is uncorrelated with the velocities of the occluding and occluded signals. For 1D image signals, such an occlusion scene can be expressed as:

$$\begin{aligned}\mathbf{I}(x,t) \;=\; & \chi(x - v_3 t)\mathbf{I}_1(x - v_1 t) \\ & - \;\chi(x - v_3 t)\mathbf{I}_2(x - v_2 t) \\ & + \;\mathbf{I}_2(x - v_2 t). \end{aligned} \tag{44}$$

As Zanker and Fleet [53, 19], we model the occlusion window with a rectangle function in the spatial coordinate as

$$\chi\left(\frac{x - x_0}{b}\right) = \begin{cases} 0 \text{ if } \left|\frac{x-x_0}{b}\right| > \frac{1}{2} \\ \frac{1}{2} \text{ if } \left|\frac{x-x_0}{b}\right| = \frac{1}{2} \\ 1 \text{ if } \left|\frac{x-x_0}{b}\right| < \frac{1}{2}. \end{cases} \tag{45}$$

Such a function has a non-zero value in the interval $[x_0 - \frac{b}{2}, x_0 + \frac{b}{2}]$ and zero otherwise. We then write the Fourier transform of the occlusion scene (8) as:

$$\begin{aligned}\mathbf{I}(k,\omega) = & \\ & K \sum_{n=-\infty}^{\infty} \operatorname{sinc}(k - nk_1) c_{1n} \delta(kv_3 - nk_1 \Delta v_3) - \\ & K \sum_{n=-\infty}^{\infty} \operatorname{sinc}(k - nk_2) c_{2n} \delta(kv_3 - nk_2 \Delta v_2) + \\ & \sum_{n=-\infty}^{\infty} c_{2n} \delta(k - nk_2, \omega + nk_2 v_2), \end{aligned} \tag{46}$$

where $\operatorname{sinc}(k) = \frac{\sin k}{k}$, $\Delta v_3 = v_3 - v1$, $\Delta v_2 = v_2 - v_1$ and the phase shift from x_0 in (45) $K = b^{-1} e^{-ikx_0 b^{-1}}$. The spectra $\delta(kv_3 + \omega - nk_1 \Delta v_3)$ and $\delta(kv_3 + \omega - nk_2 \Delta v_2)$ are consonant with the motion of the occluding window and represent a

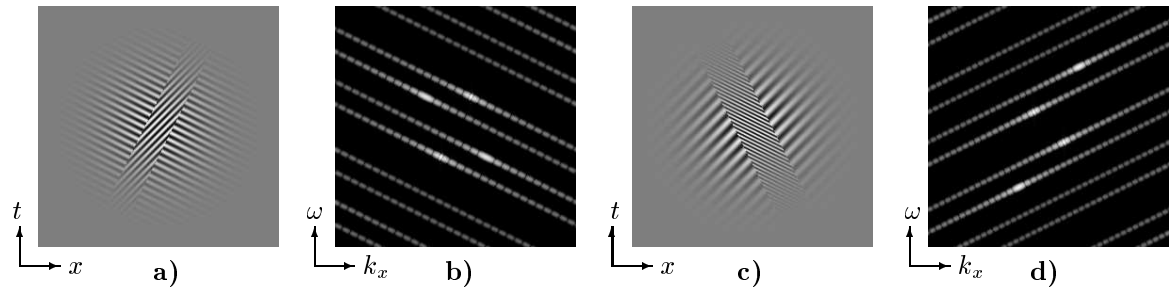

Fig. 9. Examples of Theta Motion. **a):** *Velocities of occlusion window, occluding and occluded signals are* $v_3 = 0.5$, $v_1 = 1.0$ *and* $v_2 = -2.0$ *respectively.* **b):** *Frequency spectrum of a).* **c):** *Velocities of occlusion window, occluding and occluded signals are* $v_3 = -0.5$, $v_1 = -2.0$ *and* $v_2 = 1.0$ *respectively.* **d):** *Frequency spectrum of c).*

case of Non-Fourier motion, as they do not contain the origin.

We performed two experiments with Theta motions as pictured in Figure 9. It is easily observed that the spectrum of the sinc function is convolved with each frequency of both signals and that its orientation is descriptive of the velocity of the window. As expected, the visible peaks represent the motions of both signals in the MFFC sense.

5. Conclusion

Retinal image motion and optical flow as its approximation are fundamental concepts in the field of vision. The computation of optical flow is a challenging problem as image motion includes discontinuities and multiple values mostly due to scene geometry, surface translucency and various photometric effects such as surface reflectance. In this contribution, we analyzed image motion in frequency space with respect to motion discontinuities and surface translucence. The motivation for such a study emanated from the observation that the frequency structure of occlusion, translucency and Non-Fourier motion in frequency space was not known. The results cast light on the exact structure of occlusion, translucency, Theta motion, the aperture problem and signal degeneracy for a constant model of image motion in the frequency domain with related geometrical properties.

Appendix

Proof Method of Theorem 2

The Fourier transform of the complex exponential series expansion of a 2D signal is:

$$\mathbf{I}_i(\mathbf{k}) = \int \sum_{\mathbf{n}=-\vec{\infty}}^{\vec{\infty}} c_{i\mathbf{n}} e^{i\mathbf{x}^T N\mathbf{k}_i} e^{-i\mathbf{k}^T\mathbf{x}} d\mathbf{x} = \sum_{\mathbf{n}=-\vec{\infty}}^{\vec{\infty}} c_{i\mathbf{n}} \delta(\mathbf{k} - N\mathbf{k}_i) \tag{A1}$$

and the Fourier transform of 2D step function under constant velocity is:

$$\hat{\mathbf{U}}(\mathbf{k}) = \int \mathbf{U}(\mathbf{v}_i(\mathbf{x})) e^{-i\mathbf{k}^T\mathbf{x}} d\mathbf{x} = \left(\pi\delta(\mathbf{k}) - i\frac{\delta(\mathbf{k}^T\mathbf{n}_i^{\perp})}{\mathbf{k}^T\mathbf{n}_i}\right)\delta(\mathbf{k}^T\mathbf{a}_i + \omega), \tag{A2}$$

where $\mathbf{n}_i$ is a vector normal to the occlusion boundary. Introducing (A1) and (A2) into the Fourier transform of (13) under constant velocity and solving the convolutions leads to Theorem 2.

Notes

1. Signals that are termed as degenerate have a spatially constant intensity gradient or, in other words, a unique texture orientation. This phenomenon is generally referred to as the aperture problem which arises when the Fourier spectrum of $\mathbf{I}_i(\mathbf{x})$ is concentrated on a line rather than on a plane [18, 33]. Spatiotemporally, this depicts the situation in which $\mathbf{I}_i(\mathbf{x}, t)$ exhibits a single orientation. In this case, one only obtains the speed and direction of motion normal to the orientation, noted as $\mathbf{v}_{\perp i}(\mathbf{x}, t)$. If many normal velocities are found in a single neighborhood, their respective spectra fit the plane $\mathbf{k}^T\mathbf{a}_i + \omega = 0$ from which full velocity may be obtained.
2. This assertion assumes differentiable sensor motion.

References

1. G. Adiv. Determining three-dimensional motion and structure from optical flow generated by several moving objects. *IEEE PAMI*, 7(4):384–401, 1985.
2. N. Ancona. A fast obstacle detection method based on optical flow. In *Proceedings of ECCV*, pages 267–271, Santa Mangherita Ligure, Italy, May 1992.
3. S. T. Barnard and W. B. Thompson. Disparity analysis of images. *IEEE PAMI*, 2(4):333–340, 1980.
4. J. L. Barron, D. J. Fleet, and S. S. Beauchemin. Performance of optical flow techniques. *IJCV*, 12(1):43–77, 1994.
5. J. L. Barron, A. D. Jepson, and J. K. Tsotsos. The feasibility of motion and structure from noisy time-varying image velocity information. *IJCV*, 5(3):239–269, 1990.
6. J. L. Barron and A. Liptay. Optic flow to measure minute increments in plant growth. *Bioimaging*, 2:57–61, 1994.
7. M. J. Black and P. Anandan. A model for the detection of motion over time. In *Proceedings of ICCV*, pages 33–37, Osaka, Japan, December 1990.
8. P. Bouthemy and E. Francois. Motion segmentation and qualitative dynamic scene analysis from an image sequence. *IJCV*, 10(2):159–182, 1993.
9. P. Burlina and R. Chellappa. Time-to-x: Analysis of motion through temporal parameters. In *IEEE Proceedings of CVPR*, pages 461–468, Seattle, Washington, June 1994.
10. B. Carpentieri and J. A. Storer. A split-merge parallel block-matching algorithm for video displacement estimation. In *Data Compression Conference*, pages 239–248, Snowbird, Utah, March 1992.
11. C. Chubb and G. Sperling. Drift-balanced random stimuli: A general basis for studying non-fourier motion perception. *J. Opt. Soc. Am. A*, 5(11):1986–2007, 1988.
12. V. Cornilleau-Peres and J. Droulez. Stereo correspondence from optical flow. In *Proceedings of ECCV*, pages 326–330, Antibes, France, April 1990.
13. E. Dubois. The sampling and reconstruction of time-varying imagery with application in video systems. *Proceedings of IEEE*, 73(4):502–522, 1985.
14. J. H. Duncan and T. Chou. On the detection of motion and the computation of optical flow. *IEEE PAMI*, 14(3):346–352, 1992.
15. W. Enkelmann. Obstacle detection by evaluation of optical flow fields from image sequences. In *Proceedings of ECCV*, pages 134–138, Antibes, France, April 1990.
16. I. Fermin and A. Imiya. Two-dimensional motion computation by randomized method. Technical Report TR ICS-4-6-1994, Dept. of Information and Computer Sciences, Chiba University, Japan, 1994.
17. D. J. Fleet. *Measurement of Image Velocity*. Kluwer Academic Publishers, Norwell, 1992.
18. D. J. Fleet and A. D. Jepson. Computation of component image velocity from local phase information. *IJCV*, 5(1):77–104, 1990.
19. D. J. Fleet and K. Langley. Computational analysis of non-fourier motion. *Vision Research*, 34(22):3057–3079, 1995.
20. A. Giachetti, M. Campani, and V. Torre. The use of optical flow for autonomous navigation. In *Proceedings of ECCV*, pages 146–151, Stockholm, Sweden, May 1994.
21. J. C. Hay. Optical motions and space perception: An extension of gibson's analysis. *Psychological Review*, 73(6):550–565, 1966.
22. D. J. Heeger and A. D. Jepson. Subspace methods for recovering rigid motion 2: Algorithm and implementation. *IJCV*, 7(2):95–117, 1992.
23. M. Irani, B. Rousso, and S. Peleg. Recovery of ego-motion using image stabilization. In *CVPR*, pages 454–460, Seattle, Washington, June 1994.
24. R. C. Jain. Direct computation of the focus of expansion. *IEEE PAMI*, 5(1):58–63, 1983.
25. R. C. Jain. Segmentation of frame sequences obtained by a moving observer. *IEEE PAMI*, 6(5):624–629, 1984.
26. M. R. M. Jenkin, A. D. Jepson, and J. K. Tsotsos. Techniques for disparity measurement. *CVGIP*, 53(1):14–30, 1991.
27. A. D. Jepson and M. Black. Mixture models for optical flow computation. In *IEEE Proceedings of CVPR*, pages 760–761, New York, New York, June 1993.
28. K. Langley, T. J. Atherton, R. G. Wilson, and M. H. E. Lacombe. Vertical and horizontal disparities from phase. *Image and Vision Computing*, 9(4):296–302, 1991.
29. A. Liptay, J. L. Barron, T. Jewett, and I. Van Wesenbeeck. Optic flow as an ultra-sensitive technique for measuring seedling growth in long image sequences. *J. Amer. Soc. Hort. Sci.*, 120(3):379–385, 1995.
30. H. C. Longuet-Higgins. A computer algorithm for reconstructing a scene from two projections. *Nature*, 223:133–135, 1981.
31. H. C. Longuet-Higgins and K. Prazdny. The interpretation of a moving retinal image. *Proceedings of Royal Society London*, B 208:385–397, 1980.
32. B. D. Lucas and T. Kanade. An iterative image-registration technique with an application to stereo vision. In *Proceedings of IJCAI*, pages 674–679, Vancouver, British Columbia, 1981.
33. D. Marr and S. Ullman. Directional selectivity and its use in early visual processing. *Proceedings of Royal Society London*, B 211:151–180, 1981.

34. E. De Micheli, V. Torre, and S. Uras. The accuracy of the computation of optical flow and of the recovery of motion parameters. *IEEE PAMI*, 15(5):434–447, 1993.
35. F. W. Mounts. A video encoding system using conditional picture-element replenishment. *Bell System Technical Journal*, 48:2545–2554, 1969.
36. D. W. Murray and B. F. Buxton. Scene segmentation from visual motion using global optimization. *IEEE PAMI*, 9(2):220–228, 1987.
37. H. G. Musmann, P. Pirsch, and H. J. Grallert. Advances in picture coding. *Proc of IEEE*, 73(4):523–548, 1985.
38. S. Negahdaripour and S. Lee. Motion recovery from image sequences using only first order optical flow information. *IJCV*, 9(3):163–184, 1992.
39. A. N. Netravali and J. D. Robbins. Motion compensated television coding: Part 1. *Bell System Technical Journal*, 58:631–670, 1979.
40. M. Ogata and T. Sato. Motion-detection model with two stages: Spatiotemporal filtering and feature matching. *J. Opt. Soc. Am.*, A 9(3):377–387, 1992.
41. I. Overington. Gradient-based flow segmentation and location of the focus of expansion. In *Alvey Vision Conference*, pages 860–870, University of Cambridge, England, September 1987.
42. K. Prazdny. Motion and structure from optical flow. In *Proceedings of IJCAI*, pages 702–704, Tokyo, Japan, August 1979.
43. J. L. Prince and E. R. McVeigh. Motion estimation from tagged mr image sequences. *IEEE Trans. on Medical Images*, 11(2):238–249, 1992.
44. D. Regan and K. I. Beverley. How do we avoid confounding the direction we are looking and the direction we are moving. *Science*, 215:194–196, 1982.
45. W. Reichardt, R. W. Schlogl, and M. Egelhoaf. Movement detectors of the correlation type provide sufficient information for local computation of 2d velocity fields. *Naturwissenschaften*, 75:313–315, 1988.
46. A. Rognone, M. Campani, and A. Verri. Identifying multiple motions from optical flow. In *Proceedings of ECCV*, pages 258–266, Santa Mangherita Ligue, Italy, May 1992.
47. L. A. Spacek. Edge detection and motion detection. *Image and Vision Computing*, 4(1):43–56, 1986.
48. M. Subbarao. Bounds on time-to-collision and rotational component from first-order derivatives of image flow. *CVGIP*, 50:329–341, 1990.
49. V. Sundareswaran. A fast method to estimate sensor translation. In *Proceedings of ECCV*, pages 263–267, Santa Mangherita Ligure, Italy, May 1992.
50. R. Y. Tsai and T. S. Huang. Uniqueness and estimation of three-dimensional motion parameters of rigid objects with curved surfaces. *IEEE PAMI*, 6(1):13–27, 1984.
51. R. Y. Tsai, T. S. Huang, and W. Zhu. Estimating three-dimensional motion parameters of a rigid planar patch 2: Singular value decomposition. *IEEE Trans. on Acoustics, Speech and Signal Processing*, 30(4):525–534, 1982.
52. J. D. Victor and M. M. Conte. Coherence and transparency of moving plaids composed of fourier and non-fourier gratings. *Perception & Psychophysics*, 52(4):403–414, 1988.
53. M. J. Zanker. Theta motion: A paradoxical stimulus to explore higher-order motion extraction. *Vision Research*, 33:553–569, 1993.
54. Z. Zhang and O. D. Faugeras. Three-dimensional motion computation and object segmentation in a long sequence in stereo frames. *IJCV*, 7(3), 1992.
55. H. Zheng and S. D. Blostein. An error-weighted regularization algorithm for image motion-field estimation. *IEEE Trans. on Image Processing*, 2(2):246–252, 1993.
56. Q. Zheng and R. Chellappa. Automatic feature point extraction and tracking in image sequences for unknown image motion. In *Proceedings of ICCV*, pages 335–339, Berlin, Germany, May 1993.

Steven S. Beauchemin graduated from the University of Western Ontario, London, Canada with an M.Sc. and Ph.D. in Computer Science in 1991 and 1997 respectively. He is currently an NSERC post-doctoral fellow at the University of Pennsylvania, Philadelphia, PA. His research interests include optical flow, autonomous navigation and robotics. Dr. Beauchemin was awarded the Governor General Academic Gold Medal of Canada in 1998.

John L. Barron graduated from the University of Toronto, Ontario, Canada with an M.Sc. and Ph.D. in Computer Science in 1980 and 1988 respectively. He is currently an associate professor in Computer Science at the University of Western Ontario. His research interests are in Computer Vision and include the measurement and interpretation of both optical flow and range flow and the tracking of (deformable) objects in long image sequences. Applications include measuring plant growth via optical flow and detecting and tracking severe storms in Doppler radar images.